A meshless Galerkin method with moving least square approximations for infinite elastic solids*

Li Xiao-Lin(李小林)† and Li Shu-Ling(李淑玲)

College of Mathematics Science, Chongqing Normal University, Chongqing 400047, *China*

(Received 15 January 2013; revised manuscript received 4 March 2013)

Combining moving least square approximations and boundary integral equations, a meshless Galerkin method, which is the Galerkin boundary node method (GBNM), for two- and three-dimensional infinite elastic solid mechanics problems with traction boundary conditions is discussed. In this numerical method, the resulting formulation inherits the symmetry and positive definiteness of variational problems, and boundary conditions can be applied directly and easily. A rigorous error analysis and convergence study for both displacement and stress is presented in Sobolev spaces. The capability of this method is illustrated and assessed by some numerical examples.

Keywords: meshless method, Galerkin boundary node method, error estimates, elasticity

PACS: 02.60.Cb, 02.60.Lj, 46.25.–y **DOI:** 10.1088/1674-1056/22/8/080204

1. Introduction

Meshless (or meshfree) methods have been developed and applied to a wide range of boundary value problems. Compared to the finite element method (FEM), this type of method can get rid of the difficulty of meshing and remeshing the entire structure by simply adding or deleting scattered nodes. Some meshless Galerkin methods, such as the element free Galerkin method,[1–3] the reproducing kernel particle method,[4–6] the smoothed particle hydrodynamics method,[7] and the meshless local Petrov–Galerkin method[8] have been proposed and gained noticeable progress.

As in the FEM, most works involved in the Galerkin methods mentioned above are for problems with bounded domains. In practice, however, many scientific and engineering problems are formed in infinite domains. This kind of problem includes the diffraction of water waves around an obstacle in an open sea, scattering of elastic waves by an elastic inclusion, and the problem of viscous flows around a solid body, and so forth. In numerical simulation, the unboundedness of the domain is a common difficulty.[9] In engineering treatment, the computation is usually restricted in a finite sub-domain which should be large enough. Then, the aforementioned Galerkin methods can be used to solve the new problem and obtain a numerical solution of the original problem in the bounded computational domain. Obviously, such a numerical solution is not guaranteed to converge to the true solution of the original problem in the infinite domain.

Boundary reduction is a forceful means for problems in infinite domains. In this reduction, infinite problems can be reformulated as boundary integral equations (BIEs) over the boundary of the domain. The numerical discretization of BIEs is commonly known as the boundary element method (BEM).[10,11] The BEM is powerful for infinite problems as it can reduce the dimensionality of the original problem by one. However, as for the FEM, the BEM depends on the generation of meshes, adapted or not.

The moving least squares (MLS) approximation is a well-developed scheme used to construct meshless shape functions. A variety of meshless methods[12–16] are developed by combining the MLS approximation with BIEs, such as the boundary node method (BNM)[12] and the boundary face method.[13] Because the MLS approximations lack the delta function property, boundary conditions in these methods cannot be enforced easily. The strategy used in these methods doubles the number of system equations. Recently, Cheng and Peng developed an improved MLS approximation and introduced it into BIEs to develop the boundary element-free method (BEFM).[14] Since the improved MLS approximation still lacks the delta function property, boundary conditions are implemented with constraints in the BEFM.[15]

To make the application of boundary conditions easy, a new meshless Galerkin scheme, the Galerkin boundary node method (GBNM),[17–20] has been developed by combining the weak formulations of BIEs and the MLS approximation. Compared to the aforementioned BIEs-based meshless methods, boundary conditions in the GBNM can be imposed with ease. Besides, the resulting coefficient matrices in the GBNM inherit the symmetry and positive definiteness of the variational problems. Moreover, to our knowledge the GBNM is the first BIEs-based meshless approach that has a rich mathematical foundation to justify its use. The GBNM has been applied to elastic problems in two dimensions[21] and three

*Project supported by the National Natural Science Foundation of China (Grant No. 11101454) and the Natural Science Foundation of Chongqing CSTC (Grant No. cstc2011jjA30003).

†Corresponding author. E-mail: lxlmath@163.com

© 2013 Chinese Physical Society and IOP Publishing Ltd

dimensions.[22] The results in Refs. [21] and [22] were only shown for elastic solids with displacement boundary conditions. Since the need to solve infinite elastic solids with traction boundary conditions arises in many areas of physics and engineering, this meshless Galerkin method is further developed in this paper for this kind of elastic problem in two and three dimensions simultaneously.

The following discussion begins with a deduction of variational formulation for infinite elastic solids in Section 2. The approximate cells are constructed in Section 3 for numerical integration. Section 4 gives a brief description of the MLS approximation. Section 5 presents a detailed numerical implementation and Section 6 gives the asymptotic error estimates. A comparison between GBNM, BNM, and BEM is given in Section 7. Numerical examples are provided in Section 8. Section 9 contains some conclusions.

2. Variational formulation for elastic solids

Let Ω be a bounded domain in $\mathbb{R}^d$ $(d=2,3)$ with boundary Γ and let Ω' denote the exterior of $\bar{\Omega}=\Omega\cup\Gamma$. In $\mathbb{R}^d$, a general point is denoted by $\boldsymbol{x}=(x_1,x_2,\ldots,x_d)$ or $\boldsymbol{y}=(y_1,y_2,\ldots,y_d)$.

Consider the following infinite elastic problem of solid mechanics

$$\begin{cases} \mu\Delta\boldsymbol{u}+(\lambda+\mu)\nabla(\nabla\cdot\boldsymbol{u})=0, & \text{in } \Omega', \\ T\boldsymbol{u}=g, & \text{on } \Gamma, \end{cases} \tag{1}$$

where $\boldsymbol{u}=(u_1,u_2,\ldots,u_d)$ is the unknown displacement field; $\mu>0$ and $\lambda>-\mu$ are given Lamé constants; Δ, ∇, and ∇ are the Laplacian, gradient, and divergence operators, respectively; $\boldsymbol{g}$ is a prescribed function on Γ; and T is the following conformal derivative operator

$$T\boldsymbol{u}=\lambda(\nabla\cdot\boldsymbol{u})\cdot\boldsymbol{n}+2\mu\frac{\partial\boldsymbol{u}}{\partial\boldsymbol{n}}+\mu\boldsymbol{n}\times\operatorname{curl}\boldsymbol{u},$$

where $\boldsymbol{n}$ is the outward normal direction on Γ. Besides, we append to problem (1) the following condition at infinity:[10,11]

$$\boldsymbol{u}(\boldsymbol{x})=\boldsymbol{\omega}(\boldsymbol{x})+O\left(|\boldsymbol{x}|^{1-d}\right) \quad \text{as} \quad |\boldsymbol{x}|\to\infty, \quad \boldsymbol{\omega}(\boldsymbol{x})\in\mathscr{R}$$

to be sure of the uniqueness of the solution. Here,

$$\mathscr{R}=\left\{\boldsymbol{\omega}:\boldsymbol{\omega}(\boldsymbol{x})=\begin{cases}\boldsymbol{a}+\boldsymbol{b}(-x_2,x_1)^{\mathrm{T}}, & d=2\\ \boldsymbol{a}+\boldsymbol{b}\times\boldsymbol{x}, & d=3\end{cases},\ \boldsymbol{a},\boldsymbol{b}\in\mathbb{R}^d\right\}$$

denotes the space of the rigid body motions.

The solution of problem (1) can be expressed as[11]

$$\boldsymbol{u}(\boldsymbol{x})=-\int_\Gamma\psi(\boldsymbol{y})(T_{\boldsymbol{y}}\boldsymbol{E})(\boldsymbol{x},\boldsymbol{y})\,\mathrm{d}S_{\boldsymbol{y}}+\boldsymbol{\omega}(\boldsymbol{x}), \quad \boldsymbol{x}\in\Omega', \tag{2}$$

where $\psi=(\psi_1,\psi_2,\ldots,\psi_d)$ is the jump of $\boldsymbol{u}$ across Γ, the subscript $\boldsymbol{y}$ in $T_{\boldsymbol{y}}\boldsymbol{E}$ denotes differentiations with respect to $\boldsymbol{y}$, and $\boldsymbol{E}=[E_{ij}]_{i,j=1}^d$ is the displacement of Kelvin's solution.[11]

Applying the boundary condition of problem (1), we get the following BIE

$$(D\psi)(\boldsymbol{x})=\boldsymbol{g}(\boldsymbol{x}), \quad \boldsymbol{x}\in\Gamma, \tag{3}$$

where D is the following hypersingular integral operator

$$(D\psi)(\boldsymbol{x})=-\int_\Gamma\psi(\boldsymbol{y})(T_{\boldsymbol{x}}T_{\boldsymbol{y}}\boldsymbol{E})(\boldsymbol{x},\boldsymbol{y})\,\mathrm{d}S_{\boldsymbol{y}}.$$

Let $H^\tau(\Gamma)=\left\{u|_\Gamma:u\in H^{\tau+1/2}\left(\mathbb{R}^d\right)\right\}$, $\tau\geq0$, denote the usual Sobolev space of functions defined on Γ.[10,11] Clearly, $L^2(\Gamma)=H^0(\Gamma)$. Besides, let $H^{-\tau}(\Gamma)$ be the dual space of $H^\tau(\Gamma)$ with respect to the duality $\langle\cdot,\cdot\rangle_\Gamma$ which is defined for functions w and v by $\langle w,v\rangle_\Gamma=\int_\Gamma w(\boldsymbol{y})v(\boldsymbol{y})\,\mathrm{d}S_{\boldsymbol{y}}$. The known traction function $\boldsymbol{g}$ in problem (1) needs to satisfy certain equilibrium conditions for a solution to exist. In fact, from Betti formula we obtain the necessary compatibility conditions $\langle\boldsymbol{g},\boldsymbol{\omega}\rangle_\Gamma=0$ for all $\boldsymbol{\omega}\in\mathscr{R}$. Therefore, for any $\tau\in\mathbb{R}$, let

$$\boldsymbol{H}_0^\tau(\Gamma)=\left\{\boldsymbol{g}:\boldsymbol{g}\in(H^\tau(\Gamma))^d,\langle\boldsymbol{g},\boldsymbol{\omega}\rangle_\Gamma=0 \text{ for all } \boldsymbol{\omega}\in\mathscr{R}\right\},$$
$$\bar{\boldsymbol{H}}^\tau(\Gamma)=(H^\tau(\Gamma))^d/\mathscr{R}.$$

Theorem 1[11] The BIE (3) defines an isomorphism from $\bar{\boldsymbol{H}}^{1/2}(\Gamma)$ onto $\boldsymbol{H}_0^{-1/2}(\Gamma)$ and admits a variational problem to find $\psi\in\bar{\boldsymbol{H}}^{1/2}(\Gamma)$ such that

$$\langle D\psi,\psi'\rangle_\Gamma=\langle\boldsymbol{g},\psi'\rangle_\Gamma, \quad \forall\psi'\in\bar{\boldsymbol{H}}^{1/2}(\Gamma), \tag{4}$$

in which the bilinear form $\langle D\cdot,\cdot\rangle_\Gamma$ is continuous and coercive on $\bar{\boldsymbol{H}}^{1/2}(\Gamma)$.

The variational problem (4) admits only one solution due to the Lax–Milgram theorem. However, it is not convenient to tackle directly the rigid body motions. To determine $\psi\in\boldsymbol{H}^{1/2}(\Gamma)$ in a definite manner we can add the constraint condition[10,11]

$$\langle\psi,\xi_l\rangle_\Gamma=0, \quad l=1,2,\ldots,3(d-1), \tag{5}$$

where ξ_l is the basis function of the space $\mathscr{R}$. For $d=2$, $\xi_1=(1,0)^{\mathrm{T}}$, $\xi_2=(0,1)^{\mathrm{T}}$, and $\xi_3=(-x_2,x_1)^{\mathrm{T}}$; while for $d=3$, $\xi_1=(1,0,0)^{\mathrm{T}}$, $\xi_2=(0,1,0)^{\mathrm{T}}$, $\xi_3=(0,0,1)^{\mathrm{T}}$, $\xi_4=(0,x_2,-x_3)^{\mathrm{T}}$, $\xi_5=(x_3,0,-x_1)^{\mathrm{T}}$, and $\xi_6=(-x_2,x_1,0)^{\mathrm{T}}$.

The variational problem (4) has integrations on Γ. As in many other meshless methods, an integration cell is used in the GBNM to approximate the boundary and perform integration via Gaussian quadrature, while the unknown function ψ is approximated by the MLS method based only on boundary nodes.

3. Integration cell

Suppose that the boundary Γ is the union of piecewise smooth segments called panels and can be partitioned finitely into many smooth pieces Υ_k, i.e., $\Gamma=\bigcup_{i=1}^N\Upsilon_k$. Each Υ_k can be considered to be the image of G_k by a smooth bijection φ_k, i.e., $\Upsilon_k=\varphi_k(G_k)$. In the two-dimensional case $(d=2)$, G_k is a

bounded straight segment in R, while in the three-dimensional case ($d=3$), G_k is a bounded polygonal domain in $\mathbb{R}^2$. Let T_{kh} be a subdivision of G_k by straight segments for $d=2$ and by triangles for $d=3$. On each T_{kh}, we construct the β-degree interpolant function of φ_k denoted by φ_{kh}. Let $\Upsilon_{kh}=\phi_{kh}(G_k)$ be the images of G_k by φ_{kh}, then $\Gamma_h:=\bigcup_{k=1}^{N}\Upsilon_{kh}$ is the desired integration cell. Clearly, Γ_h is a connected parametric curve or surface of degree β.

In meshless methods, the number of nodes corresponding to each cell is arbitrary. However, to perform accurate numerical integration, it is recommended to use a small number of nodes per cell.[12,17–20] Previous works demonstrated that one node per cell and the position of the node at the centroid of the cell can yield excellent results. In this study, one boundary node $\boldsymbol{x}_i$ is selected at the centroid of the cell Γ_i. Therefore, we have N boundary nodes $\{\boldsymbol{x}_i\}_{i=1}^{N}$.

4. The moving least squares (MLS) scheme

The MLS approximation for a function v is defined by[23–25]

$$v(\boldsymbol{x})\approx\mathscr{M}v(\boldsymbol{x})=\sum_{i=1}^{N}\boldsymbol{\Phi}_i(\boldsymbol{x})v_i,\quad \boldsymbol{x}\in\Gamma,$$

where $\mathscr{M}$ is an approximation operator, and

$$\boldsymbol{\Phi}_i(\boldsymbol{x})=\begin{cases}\sum_{j=0}^{\ell}P_j(\boldsymbol{s})\left[\boldsymbol{A}^{-1}(\boldsymbol{s})\boldsymbol{B}(\boldsymbol{s})\right]_{jk}, & i=I_k\in\wedge(\boldsymbol{s})\\ 0, & i\notin\wedge(\boldsymbol{s}),\end{cases}\quad 1\le i\le N,$$

is the MLS shape function, s is a local coordinate of $\boldsymbol{x}$ on Γ, $\boldsymbol{A}(s)=\sum_{k\in\wedge(\boldsymbol{x}(s))}w_k(s)\boldsymbol{P}(s_k)\boldsymbol{P}^{\mathrm{T}}(s_k)$, $\boldsymbol{B}(s)=[w_{I_1}(s)\boldsymbol{P}(s_{I_1}),w_{I_2}(s)\boldsymbol{P}(s_{I_2}),\cdots,w_{I_\kappa}(s)\boldsymbol{P}(s_{I_\kappa})]$, $\wedge(\boldsymbol{x})=\{I_1,I_2,\ldots,I_\kappa\}$ is the set of the global sequence numbers of boundary nodes in the influence domain of $\boldsymbol{x}$, $\boldsymbol{P}(s)$ is a vector of the polynomial basis, $\ell+1$ is the number of monomials in the polynomial basis, and w_k is a nonnegative weight function. In what follows, we assume that there is a nonnegative integer γ such that w_k is γ-times continuously differentiable. Then we have:[17,19]

Proposition 1 Let $\Re_i$ be the influence domain of $\boldsymbol{x}_i$, then $\boldsymbol{\Phi}_i(\mathbf{x})\in C_0^{\min(\gamma,\beta)}(\Re_i)$, $1\le i\le N$.

Under appropriate assumptions on nodes and MLS shape functions, Cheng and Cheng obtained error estimates of the MLS scheme in $W^{k,p}$.[23] Recently, with weaker suppositions on nodes and weight functions, Li and Zhu obtained the following estimates in H^k.[17,19]

Theorem 2 For any $v\in H^{m+1}(\Gamma)$, we have

$$\|v-\mathscr{M}v\|_{H^k(\Gamma)}\le Ch^{\gamma+1-k}\|v\|_{H^{\gamma+1}(\Gamma)},\quad 0\le k\le m\le\gamma,$$

where h is the nodal spacing.

5. Approximation and discretization

In the presented GBNM, the MLS approximation is used for generating the meshless approximate space. Based on the MLS approximation, Cheng and Li developed a new approximation scheme — the complex variable moving least-squares (CVMLS) approximation in which the trial function of a two-dimensional problem is formed with a one-dimensional basis function.[24,25] The CVMLS approximation has been inserted into the element-free Galerkin method and the BEFM.[26–31] The CVMLS approximation can also be used in the GBNM.

Let $\boldsymbol{V}_h(\Gamma_h)=(\mathrm{span}\{\Phi_i,1\le i\le N\})^d$. For tackling the rigid body motions, let $\bar{\boldsymbol{V}}_h(\Gamma_h)=\boldsymbol{V}_h(\Gamma_h)/\mathscr{R}$. Then, variational problem (4) is approximated as

$$\left\langle D\psi_h,\psi_h'\right\rangle_{\Gamma_h}=\left\langle \boldsymbol{g}_h,\psi_h'\right\rangle_{\Gamma_h},\quad\forall\psi_h'\in\bar{\boldsymbol{V}}_h(\Gamma_h),\tag{6}$$

where $\boldsymbol{g}_h$ is an approximation of $\boldsymbol{g}$ restricted on Γ_h. In computations, one can determine $\boldsymbol{g}_h$ as an interpolation of $\boldsymbol{g}$ with basis functions of piecewise polynomial degree β, and then[12,13]

$$\|\boldsymbol{g}-\tilde{\boldsymbol{g}}_h\|_{\boldsymbol{H}_0^k(\Gamma)}\le Ch^{m-k}\|\boldsymbol{g}\|_{\boldsymbol{H}_0^m(\Gamma)},\tag{7}$$

where $0\le k\le m\le\beta+1$,

$$\tilde{\boldsymbol{g}}_h(\boldsymbol{x})=\left(\boldsymbol{g}_h\circ\Psi^{-1}\right)(\boldsymbol{x})\cdot J(\partial\Psi)(\boldsymbol{x}),$$

Ψ is an orthogonal projection mapping of Γ onto Γ_h and J is the Jacobian by Ψ.

Once ψ_h is found from variational problem (6), the approximate solution $\boldsymbol{u}_h$ of the elastic problem (1) can be computed from an approximation of Eq. (2), i.e.,

$$\begin{aligned}\boldsymbol{u}_h(\boldsymbol{x}) &= -\int_{\Gamma_h}\psi_h(\boldsymbol{y})(T_{\boldsymbol{y}}\boldsymbol{E})(\boldsymbol{x},\boldsymbol{y})\,\mathrm{d}S_{\boldsymbol{y}}\\ &\quad+\boldsymbol{\omega}(\boldsymbol{x}),\quad \boldsymbol{x}\in\Omega'.\end{aligned}\tag{8}$$

To prove variational problem (6) has a unique solution, we need the following lemma.

Lemma 1 For any $\psi_h,\psi'_h\in\bar{\boldsymbol{V}}_h(\Gamma_h)$, let $\tilde{\psi}_h=\psi_h\circ\Psi^{-1}$ and $\tilde{\psi}'_h=\psi'_h\circ\Psi^{-1}$, then

$$\begin{aligned}&\left|\left\langle D\tilde{\psi}_h,\tilde{\psi}'_h\right\rangle_{\Gamma}-\left\langle D\psi_h,\psi'_h\right\rangle_{\Gamma_h}\right|\\ &\le Ch^{\beta+1}\|\tilde{\psi}_h\|_{\bar{\boldsymbol{H}}^{1/2}(\Gamma)}\left\|\tilde{\psi}'_h\right\|_{\bar{\boldsymbol{H}}^{1/2}(\Gamma)}.\end{aligned}$$

Proof With Theorem 5.7 of Ref. [11], we can prove

$$\begin{aligned}&|(T_{\boldsymbol{x}}T_{\boldsymbol{y}}\boldsymbol{E})(\boldsymbol{x},\boldsymbol{y})-(T_{\boldsymbol{x}}T_{\boldsymbol{y}}\boldsymbol{E})(\Psi(\boldsymbol{x}),\Psi(\boldsymbol{y}))|\\ &\le Ch^{\beta+1}/|\boldsymbol{x}-\boldsymbol{y}|^3,\\ &|(T_{\boldsymbol{x}}T_{\boldsymbol{y}}\boldsymbol{E})(\boldsymbol{x},\boldsymbol{y})|\le C/|\boldsymbol{x}-\boldsymbol{y}|^3,\\ &|1-J(\partial\Psi)(\boldsymbol{x})\cdot J(\partial\Psi)(\boldsymbol{y})|\le Ch^{\beta+1},\end{aligned}$$

and $|J(\partial\Psi)(\boldsymbol{x})|\le C$. Thus,

$$\begin{aligned}&|(T_{\boldsymbol{x}}T_{\boldsymbol{y}}\boldsymbol{E})(\boldsymbol{x},\boldsymbol{y})-(T_{\boldsymbol{x}}T_{\boldsymbol{y}}\boldsymbol{E})(\Psi(\boldsymbol{x}),\Psi(\boldsymbol{y}))\\ &\times J(\partial\Psi)(\boldsymbol{x})J(\partial\Psi)(\boldsymbol{y})|\end{aligned}$$

$$
\begin{aligned}
&= |(T_{\boldsymbol{x}}T_{\boldsymbol{y}}\boldsymbol{E})(\boldsymbol{x},\boldsymbol{y})\cdot[1-J(\partial\Psi)(\boldsymbol{x})\cdot J(\partial\Psi)(\boldsymbol{y})] \\
&\quad + [(T_{\boldsymbol{x}}T_{\boldsymbol{y}}\boldsymbol{E})(\boldsymbol{x},\boldsymbol{y})-(T_{\boldsymbol{x}}T_{\boldsymbol{y}}\boldsymbol{E})(\Psi(\boldsymbol{x}),\Psi(\boldsymbol{y}))] \\
&\quad \times J(\partial\Psi)(\boldsymbol{x})J(\partial\Psi)(\boldsymbol{y})| \\
&\le Ch^{\beta+1}/|\boldsymbol{x}-\boldsymbol{y}|^3.
\end{aligned}
$$

Accordingly, by changing the integrals in $\langle D\psi_h,\psi'_h\rangle_{\Gamma_h}$ into integrals on Γ by Ψ we get

$$
\begin{aligned}
&\left|\left\langle D\tilde{\psi}_h,\tilde{\psi}'_h\right\rangle_{\Gamma}-\langle D\psi_h,\psi'_h\rangle_{\Gamma_h}\right| \\
&= \left|-\int_{\Gamma}\int_{\Gamma}\tilde{\psi}_h(\boldsymbol{x})\,\tilde{\psi}'_h(\boldsymbol{y})\,[(T_{\boldsymbol{x}}T_{\boldsymbol{y}}\boldsymbol{E})(\boldsymbol{x},\boldsymbol{y}) \right. \\
&\quad -(T_{\boldsymbol{x}}T_{\boldsymbol{y}}\boldsymbol{E})(\Psi(\boldsymbol{x}),\Psi(\boldsymbol{y})) \\
&\quad \left.\times J(\partial\Psi)(\boldsymbol{x})J(\partial\Psi)(\boldsymbol{y})]\mathrm{d}S_{\boldsymbol{x}}\mathrm{d}S_{\boldsymbol{y}}\right| \\
&\le Ch^{\beta+1}\int_{\Gamma}\int_{\Gamma}\left|\tilde{\psi}_h(\boldsymbol{x})\,\tilde{\psi}'_h(\boldsymbol{y})\right|/|\boldsymbol{x}-\boldsymbol{y}|^3\mathrm{d}S_{\boldsymbol{x}}\mathrm{d}S_{\boldsymbol{y}} \\
&\le Ch^{\beta+1}\|\tilde{\psi}_h\|_{\tilde{\boldsymbol{H}}^{1/2}(\Gamma)}\left\|\tilde{\psi}'_h\right\|_{\tilde{\boldsymbol{H}}^{1/2}(\Gamma)}.
\end{aligned}
$$

Theorem 3 Variational problem (6) has one and only one solution.

Proof Using Lemma 1 and the coerciveness of $\langle D\cdot,\cdot\rangle_{\Gamma}$ yields

$$
\begin{aligned}
\langle D\psi_h,\psi_h\rangle_{\Gamma_h} &\ge \langle D\tilde{\psi}_h,\tilde{\psi}_h\rangle_{\Gamma}-Ch^{\beta+1}\|\tilde{\psi}_h\|^2_{\tilde{\boldsymbol{H}}^{1/2}(\Gamma)} \\
&\ge C\|\tilde{\psi}_h\|^2_{\tilde{\boldsymbol{H}}^{1/2}(\Gamma)}-Ch^{\beta+1}\|\tilde{\psi}_h\|^2_{\tilde{\boldsymbol{H}}^{1/2}(\Gamma)} \\
&\ge C\left(1-h^{\beta+1}\right)\|\tilde{\psi}_h\|^2_{\tilde{\boldsymbol{H}}^{1/2}(\Gamma)}. \qquad (9)
\end{aligned}
$$

Therefore, the proof is complete by the Lax–Milgram theorem.

In light of Eq. (5), the solution ψ_h of variational problem (6) should satisfy the following constraint condition

$$
\langle\psi_h,\xi_l\rangle_{\Gamma_h}=0,\quad l=1,2,\ldots,3(d-1). \qquad (10)
$$

To tackle this condition, one can solve the discrete equations of problem (6) and Eq. (10) simultaneously by the least square method. This strategy will lose the symmetry. To maintain the symmetry and positive definiteness of problem (6), we formulate an extended variational problem, along the lines as in Ref. [19], to find $\psi_h\in\boldsymbol{V}_h(\Gamma_h)$ such that

$$
\begin{aligned}
&\left\langle D\psi_h,\psi'_h\right\rangle_{\Gamma_h}+\sum_{l=1}^{3(d-1)}\langle\psi_h,\xi_l\rangle_{\Gamma_h}\left\langle\psi'_h,\xi_l\right\rangle_{\Gamma_h} \\
&=\left\langle g_h,\psi'_h\right\rangle_{\Gamma_h},\quad \forall\psi'_h\in\boldsymbol{V}_h(\Gamma_h). \qquad (11)
\end{aligned}
$$

It can be verified that variational problems (6) and (11) are equivalent.

Now, the discrete equations of the GBNM for infinite elastic solid mechanics problems are deduced using variational problem (11). On $\boldsymbol{V}_h(\Gamma_h)$, the approximate solution $\psi_h=(\psi_{1h},\psi_{2h},\ldots,\psi_{dh})$ can be written as

$$
\psi_{ih}(\boldsymbol{y})=\sum_{m=1}^{N}\Phi_m(\boldsymbol{y})\,\psi_i^{(m)},\quad \boldsymbol{y}\in\Gamma. \qquad (12)
$$

Substituting Eq. (12) into variational problem (11), in light of Proposition 1, one can get the following linear systems. In the two-dimensional case ($d=2$),

$$
\begin{aligned}
&\left(\begin{Bmatrix}[a_{km}^{11}][a_{km}^{12}]\\ [a_{km}^{21}][a_{km}^{22}]\end{Bmatrix}+\begin{Bmatrix}[c_{km}^{11}][c_{km}^{12}]\\ [c_{km}^{21}][c_{km}^{22}]\end{Bmatrix}\right)\begin{pmatrix}\{\psi_1^{(m)}\}\\ \{\psi_2^{(m)}\}\end{pmatrix} \\
&=\begin{pmatrix}\{f_k^1\}\\ \{f_k^2\}\end{pmatrix}, \qquad (13)
\end{aligned}
$$

while in the three-dimensional case ($d=3$),

$$
\begin{aligned}
&\left(\begin{Bmatrix}[a_{km}^{11}][a_{km}^{12}][a_{km}^{13}]\\ [a_{km}^{21}][a_{km}^{22}][a_{km}^{23}]\\ [a_{km}^{31}][a_{km}^{32}][a_{km}^{33}]\end{Bmatrix}+\begin{Bmatrix}[c_{km}^{11}][c_{km}^{12}][c_{km}^{13}]\\ [c_{km}^{21}][c_{km}^{22}][c_{km}^{23}]\\ [c_{km}^{31}][c_{km}^{32}][c_{km}^{33}]\end{Bmatrix}\right) \\
&\times\begin{pmatrix}\{\psi_1^{(m)}\}\\ \{\psi_2^{(m)}\}\\ \{\psi_3^{(m)}\}\end{pmatrix}=\begin{pmatrix}\{f_k^1\}\\ \{f_k^2\}\\ \{f_k^3\}\end{pmatrix}. \qquad (14)
\end{aligned}
$$

In Eqs. (13) and (14), $k,m=1,2,\cdots,N$, and

$$
\begin{aligned}
a_{km}^{ij} &= -\int_{\Re_k}\int_{\Re_m}\Phi_m(\boldsymbol{x})\,\Phi_k(\boldsymbol{y})\,(T_{\boldsymbol{x}}T_{\boldsymbol{y}}E_{ij})(\boldsymbol{x},\boldsymbol{y})\,\mathrm{d}S_{\boldsymbol{x}}\mathrm{d}S_{\boldsymbol{y}}, \\
&\quad i,j=1,2,\ldots,d, \\
c_{km}^{ij} &= \sum_{l=1}^{3(d-1)}c_k^jc_m^i,\quad c_k^j=\int_{\Re_k}\Phi_k(\boldsymbol{y})\,\xi_{jl}(\boldsymbol{y})\,\mathrm{d}S_{\boldsymbol{y}}, \\
&\quad i,j=1,2,\ldots,d, \\
f_k^j &= \int_{\Re_k}g_{jh}(\boldsymbol{y})\,\Phi_k(\boldsymbol{y})\,\mathrm{d}S_{\boldsymbol{y}}, \\
&\quad j=1,2,\ldots,d,
\end{aligned}
$$

where $\Re_k$ and $\Re_m$ are, respectively, the influence domain of the boundary nodes $\boldsymbol{x}_k$ and $\boldsymbol{x}_m$, and are parts of the integration cell Γ_h.

It can be found that $\left[a_{km}^{ij}\right]=\left[a_{km}^{ji}\right]$ and each block matrix $\left[a_{km}^{ij}\right]$ is symmetric, thus there are only $d\cdot N(N+1)$ entries a_{km}^{ij} that need to be calculated. Besides, we can observe that $c_{km}^{ij}=c_{mk}^{ji}$ and there have $d+1$ different nonzero entries ξ_{jl} in the sense of absolute value, hence the calculation of all entries c_{km}^{ij} requires the calculation of $(d+1)N$ entries c_k^j only.

From the above analysis, one can see that the boundary function is multiplied by MLS shape functions and integrated over the boundary. Although MLS approximations lack the delta function property, no additional equations are used in the present method for imposing boundary conditions.

6. Error estimates

Theorem 4 Let ψ and ψ_h be the solutions of variational problems (4) and (6), respectively. Suppose that $\boldsymbol{g}\in\boldsymbol{H}_0^{\beta+1}(\Gamma)$ and $\psi\in\tilde{\boldsymbol{H}}^{m+1}(\Gamma)$ with $1/2\le m\le\gamma\le\beta$, then

$$
\|\psi-\tilde{\psi}_h\|_{\tilde{\boldsymbol{H}}^{-k}(\Gamma)}
$$

$$\leq C\Big[h^{m+k+1}\|\psi\|_{\tilde{\boldsymbol{H}}^{m+1}(\Gamma)} + h^{\beta+1}\left(h^{k+1}\|\boldsymbol{g}\|_{\boldsymbol{H}_0^{\beta+1}(\Gamma)} + \|\psi\|_{\tilde{\boldsymbol{H}}^{1/2}(\Gamma)}\right)\Big], \quad (15)$$

where $\tilde{\psi}_h = \psi_h \circ \Psi^{-1}$ and $-1/2 \leq k \leq \gamma$.

Proof From $\mathscr{M}\psi \circ \Psi \in \tilde{\boldsymbol{V}}_h(\Gamma_h)$ it follows that

$$\begin{aligned}
&\langle D(\psi_h - \mathscr{M}\psi\circ\Psi), \psi_h - \mathscr{M}\psi\circ\Psi\rangle_{\Gamma_h} \\
=\ &\langle \tilde{g}_h - \boldsymbol{g}, \tilde{\psi}_h - \mathscr{M}\psi\rangle_{\Gamma_h} + \langle D(\psi - \mathscr{M}\psi), \tilde{\psi}_h - \mathscr{M}\psi\rangle_{\Gamma} \\
&+ \langle D(\mathscr{M}\psi), \tilde{\psi}_h - \mathscr{M}\psi\rangle_{\Gamma} \\
&- \langle D(\mathscr{M}\psi\circ\Psi), \psi_h - \mathscr{M}\psi\circ\Psi\rangle_{\Gamma_h}.
\end{aligned}$$

Then, according to Eq. (9), Lemma 1, and the continuity of $\langle D\cdot,\cdot\rangle_{\Gamma}$, we obtain

$$\begin{aligned}
&\|\tilde{\psi}_h - \mathscr{M}\psi\|_{\tilde{\boldsymbol{H}}^{1/2}(\Gamma)} \\
\leq\ & C\big\{\|\boldsymbol{g} - \tilde{g}_h\|_{\boldsymbol{H}_0^{-1/2}(\Gamma)} + \|\psi - \mathscr{M}\psi\|_{\tilde{\boldsymbol{H}}^{1/2}(\Gamma)} \\
&+ h^{\beta+1}\|\mathscr{M}\psi\|_{\tilde{\boldsymbol{H}}^{1/2}(\Gamma)}\big\}.
\end{aligned}$$

So, applying Theorem 2 and Eq. (7) yields

$$\begin{aligned}
&\|\psi - \tilde{\psi}_h\|_{\tilde{\boldsymbol{H}}^{1/2}(\Gamma)} \\
\leq\ & \|\psi - \mathscr{M}\psi\|_{\tilde{\boldsymbol{H}}^{1/2}(\Gamma)} + \|\mathscr{M}\psi - \tilde{\psi}_h\|_{\tilde{\boldsymbol{H}}^{1/2}(\Gamma)} \\
\leq\ & C\big\{\|\boldsymbol{g} - \tilde{g}_h\|_{\boldsymbol{H}_0^{-1/2}(\Gamma)} + \|\psi - \mathscr{M}\psi\|_{\tilde{\boldsymbol{H}}^{1/2}(\Gamma)} \\
&+ h^{\beta+1}\|\mathscr{M}\psi\|_{\tilde{\boldsymbol{H}}^{1/2}(\Gamma)}\big\} \\
\leq\ & C\big\{h^{\beta+3/2}\|\boldsymbol{g}\|_{\boldsymbol{H}_0^{\beta+1}(\Gamma)} \\
&+ h^{m+3/2}\|\psi\|_{\tilde{\boldsymbol{H}}^{m+1}(\Gamma)} + h^{\beta+1}\|\psi\|_{\tilde{\boldsymbol{H}}^{1/2}(\Gamma)}\big\}, \quad (16)
\end{aligned}$$

which shows Eq. (15) for $k = -1/2$.

Let $\boldsymbol{w} = D^{-1}\boldsymbol{g}$, then using Theorem 1 leads to

$$\begin{aligned}
&\|\psi - \tilde{\psi}_h\|_{\tilde{\boldsymbol{H}}^{-\gamma}(\Gamma)} \\
=\ & \sup_{\boldsymbol{g}\in\boldsymbol{H}_0^{\gamma}(\Gamma)} \frac{\langle \psi - \tilde{\psi}_h, \boldsymbol{g}\rangle_{\Gamma}}{\|\boldsymbol{g}\|_{\boldsymbol{H}_0^{\gamma}(\Gamma)}} \\
\leq\ & C \sup_{\boldsymbol{w}\in\tilde{\boldsymbol{H}}^{\gamma+1}(\Gamma)} \frac{\langle D(\psi - \tilde{\psi}_h), \boldsymbol{w}\rangle_{\Gamma}}{\|\boldsymbol{w}\|_{\tilde{\boldsymbol{H}}^{\gamma+1}(\Gamma)}}. \quad (17)
\end{aligned}$$

Now, we have

$$\begin{aligned}
&\langle D(\psi - \tilde{\psi}_h), \boldsymbol{w}\rangle_{\Gamma} \\
=\ & \langle D(\psi - \tilde{\psi}_h), \boldsymbol{w} - \mathscr{M}\boldsymbol{w}\rangle_{\Gamma} \\
&+ \langle D\psi, \mathscr{M}\boldsymbol{w}\rangle_{\Gamma} - \langle D\tilde{\psi}_h, \mathscr{M}\boldsymbol{w}\rangle_{\Gamma}. \quad (18)
\end{aligned}$$

Applying Eq. (16) and Theorem 2, we get

$$\begin{aligned}
&\langle D(\psi - \tilde{\psi}_h), \boldsymbol{w} - \mathscr{M}\boldsymbol{w}\rangle_{\Gamma} \\
\leq\ & C\|\psi - \mathscr{M}\psi\|_{\tilde{\boldsymbol{H}}^{1/2}(\Gamma)}\|\boldsymbol{w} - \mathscr{M}\boldsymbol{w}\|_{\tilde{\boldsymbol{H}}^{1/2}(\Gamma)} \\
\leq\ & Ch^{\gamma+1/2}\big\{h^{\beta+3/2}\|\boldsymbol{g}\|_{\boldsymbol{H}_0^{\beta+1}(\Gamma)} + h^{m+3/2}\|\psi\|_{\tilde{\boldsymbol{H}}^{m+1}(\Gamma)} \\
&+ h^{\beta+1}\|\psi\|_{\tilde{\boldsymbol{H}}^{1/2}(\Gamma)}\big\}\|\boldsymbol{w}\|_{\tilde{\boldsymbol{H}}^{\gamma+1}(\Gamma)}. \quad (19)
\end{aligned}$$

Besides, according to Lemma 1, we obtain

$$\begin{aligned}
&\langle D\psi, \mathscr{M}\boldsymbol{w}\rangle_{\Gamma} - \langle D\tilde{\psi}_h, \mathscr{M}\boldsymbol{w}\rangle_{\Gamma} \\
=\ & \langle \boldsymbol{g}, \mathscr{M}\boldsymbol{w}\rangle_{\Gamma} - \langle \tilde{g}_h, \mathscr{M}\boldsymbol{w}\rangle_{\Gamma} + \langle D\tilde{\psi}_h, \mathscr{M}\boldsymbol{w}\circ\Psi\rangle_{\Gamma_h} \\
&- \langle D\tilde{\psi}_h, \mathscr{M}\boldsymbol{w}\rangle_{\Gamma} \\
\leq\ & C\|\boldsymbol{g} - \tilde{g}_h\|_{\boldsymbol{H}_0^{-\gamma-1}(\Gamma)}\|\mathscr{M}\boldsymbol{w}\|_{\tilde{\boldsymbol{H}}^{\gamma+1}(\Gamma)} \\
&+ Ch^{\beta+1}\|\tilde{\psi}_h\|_{\tilde{\boldsymbol{H}}^{1/2}(\Gamma)}\|\mathscr{M}\boldsymbol{w}\|_{\tilde{\boldsymbol{H}}^{1/2}(\Gamma)} \\
\leq\ & Ch^{\beta+1}\left\{h^{\gamma+1}\|\boldsymbol{g}\|_{\boldsymbol{H}_0^{\beta+1}(\Gamma)} + \|\psi\|_{\tilde{\boldsymbol{H}}^{1/2}(\Gamma)}\right\} \\
&\times \|\boldsymbol{w}\|_{\tilde{\boldsymbol{H}}^{\gamma+1}(\Gamma)}. \quad (20)
\end{aligned}$$

By inserting Eqs. (18)–(20) into Eq. (17) we can prove Eq. (15) for $k = \gamma$. For the remaining case $-1/2 < k < \gamma$, an interpolation between the obtained inequalities yields the desired result.

Theorem 5 Let $\boldsymbol{u}(\boldsymbol{x})$ and $\boldsymbol{u}_h(\boldsymbol{x})$ be given by Eqs. (2) and (8), respectively. Then there exists a constant $\delta > 0$, for any $\boldsymbol{x} \in \Omega'$ with $d_{\boldsymbol{x}} := \min_{\boldsymbol{y}\in\Gamma}|\boldsymbol{x} - \boldsymbol{y}| \geq \delta$, we have

$$\begin{aligned}
&\left|\partial^{\boldsymbol{\lambda}}\boldsymbol{u}(\boldsymbol{x}) - \partial^{\boldsymbol{\lambda}}\boldsymbol{u}_h(\boldsymbol{x})\right| \\
\leq\ & C_{(\boldsymbol{x},\boldsymbol{\lambda})}\Big[h^{m+\gamma+1}\|\psi\|_{\tilde{\boldsymbol{H}}^{m+1}(\Gamma)} \\
&+ h^{\beta+1}\left(h^{\gamma+1}\|\boldsymbol{g}\|_{\boldsymbol{H}_0^{\beta+1}(\Gamma)} + \|\psi\|_{\tilde{\boldsymbol{H}}^{1/2}(\Gamma)}\right)\Big],
\end{aligned}$$

where $C_{(\boldsymbol{x},\boldsymbol{\lambda})} = C\sum_{j=0}^{\gamma}(d_{\boldsymbol{x}})^{-j-|\boldsymbol{\lambda}|-2}$ and $\boldsymbol{\lambda} = (\lambda_1, \lambda_2, \ldots, \lambda_d)$ with non-negative integers λ_i.

Proof According to Eqs. (2) and (8) we have

$$\begin{aligned}
&|\boldsymbol{u}(\boldsymbol{x}) - \boldsymbol{u}_h(\boldsymbol{x})| \\
=\ & \left|\int_{\Gamma}\Big\{\psi(\boldsymbol{y})(T_{\boldsymbol{y}}\boldsymbol{E})(\boldsymbol{x},\boldsymbol{y}) \right. \\
&\left. - \tilde{\psi}_h(\boldsymbol{y})(T_{\boldsymbol{y}}\boldsymbol{E})(\boldsymbol{x},\Psi(\boldsymbol{y}))\cdot J(\partial\Psi)\Big\}\mathrm{d}S_{\boldsymbol{y}}\right| \\
\leq\ & C\big\{\|\psi(\boldsymbol{y}) - \tilde{\psi}_h(\boldsymbol{y})\|_{\tilde{\boldsymbol{H}}^{-\gamma}(\Gamma)}\|(T_{\boldsymbol{y}}\boldsymbol{E})(\boldsymbol{x},\boldsymbol{y})\|_{\boldsymbol{H}^{\gamma}(\Gamma)} \\
&+ \|(T_{\boldsymbol{y}}\boldsymbol{E})(\boldsymbol{x},\boldsymbol{y}) - (T_{\boldsymbol{y}}\boldsymbol{E})(\boldsymbol{x},\Psi(\boldsymbol{y}))\|_{\boldsymbol{H}^0(\Gamma)} \\
&\times \|\tilde{\psi}_h(\boldsymbol{y})\|_{\boldsymbol{H}^0(\Gamma)}\big\} + \big\{\|(T_{\boldsymbol{y}}\boldsymbol{E})(\boldsymbol{x},\Psi(\boldsymbol{y})) \\
&\times (1 - J(\partial\Psi)(\boldsymbol{y}))\|_{\boldsymbol{H}^0(\Gamma)}\|\tilde{\psi}_h(\boldsymbol{y})\|_{\boldsymbol{H}^0(\Gamma)}\big\}. \quad (21)
\end{aligned}$$

Since $d_{\boldsymbol{x}} \geq \delta > 0$, we get $\|(T_{\boldsymbol{y}}\boldsymbol{E})(\boldsymbol{x},\boldsymbol{y})\|_{\boldsymbol{H}^{\gamma}(\Gamma)} \leq C_{(\boldsymbol{x},\boldsymbol{0})}$. Besides, using Theorem 5.7 of Ref. [13] yields

$$|(T_{\boldsymbol{y}}\boldsymbol{E})(\boldsymbol{x},\boldsymbol{y}) - (T_{\boldsymbol{y}}\boldsymbol{E})(\boldsymbol{x},\Psi(\boldsymbol{y}))| \leq Ch^{\beta+1}(d_{\boldsymbol{x}})^{-3}$$

and

$$|(T_{\boldsymbol{y}}\boldsymbol{E})(\boldsymbol{x},\Psi(\boldsymbol{y}))\cdot(1 - J(\partial\Psi)(\boldsymbol{x}))| \leq Ch^{\beta+1}(d_{\boldsymbol{x}})^{-2}.$$

Consequently, by inserting these inequalities into Eq. (21) and using Theorem 4 we can prove the desired inequality for $|\boldsymbol{\lambda}| = 0$. Other cases are similar.

Theorem 5 shows that extremely high accuracy can be achieved not only for the $\boldsymbol{u}$ but also for its derivatives. Therefore, contrary to the case of the domain-type Galerkin methods, errors of stress $\boldsymbol{\sigma}$ and displacement $\boldsymbol{u}$ in the present

method are all of the same order. Besides, Theorems 4 and 5 indicate that the errors of the GBNM come from two terms: one from the approximation of the unknown function by the MLS scheme, and another from the approximation of the boundary by the integration cell. These statements are confirmed by numerical experiments.

7. Comparison between GBNM, BNM, and BEM

A comparison between the GBNM, the BNM, and the BEM is summarized concisely in Table 1. It can be observed that these methods are all based on BIEs. The difference is in the means of implementation. Compared with the BEM, the GBNM alleviates the difficulty of meshing and remeshing the entire boundary structure via simply adding or deleting boundary nodes. Compared with the BNM, the GBNM conserves the symmetry and positive definiteness of variational problems in the process of numerical implementation. Besides, the number of system equations and the number of unknowns in the BNM are double those in the GBNM.

Table 1. Comparison between the GBNM, the BNM, and the BEM.

	GBNM	BNM	BEM
Mesh	no	no	yes
Approximation/Interpolation	MLS	MLS	polynomial
Interpolation domain based on	distributed nodes	distributed nodes	pre-defined elements
Delta property of shape function	no	no	yes
Imposing boundary conditions	easy	difficult	easy
Number of system equations or number of unknowns for 3D elasticity with N boundary nodes	$3N$	$6N$	$3N$
Symmetry and positive definiteness of system equations	yes	no	no for collocation BEM; yes for Galerkin BEM
Convergence proof	some	absent	few for collocation BEM; much for Galerkin BEM

8. Numerical experiments

To demonstrate the validity of the proposed Galerkin method and to confirm the theoretical error estimates, some numerical experiments are presented for infinite elastic solids. In all computations, unless indicated otherwise, a quadratic geometric representation is used for each cell, that is $\beta = 2$.

8.1. Infinite plate with a circular hole

Consider an infinite plate with a unit central hole. The plate is subjected to a uniform tension, $\sigma_0 = 1$, in the x_1 direction at infinity. Figure 1 depicts the sketched geometric configuration and the distribution of boundary nodes. In the computation, the traction boundary conditions given by the exact solutions are imposed on the boundary. Besides, a plane stress case with Young's modulus $E = 10$ and Poisson's ratio $\nu = 0.3$ is considered.

The numerical results for the stress σ_{11} on the vertical centerline are shown in Fig. 2 together with the analytical solutions, while the stress σ_{22} on the horizontal centerline is given in Fig. 3. In this analysis, we applied 32 regularly distributed nodes on the circular boundary. From these figures, it can be observed that the numerical solutions are in excellent agreement with the exact solutions.

Numerical results with random distributed nodes are also plotted in Figs. 2 and 3. In this analysis, random nodes are generated via adding a random perturbation of value $0.20h$ to the uniform node distribution. Comparing two cases for random and uniformly spaced nodes, it can be found that the difference between their results is small.

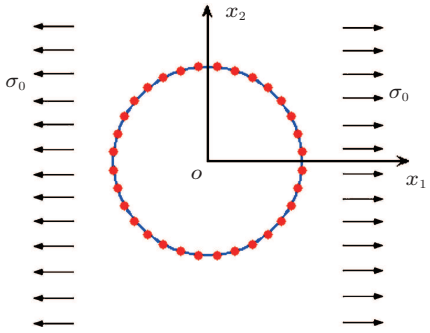


Fig. 1. (color online) Infinite plate with a circular hole (the dot represents boundary nodes).

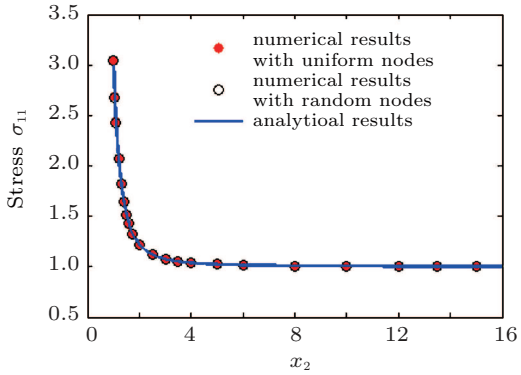


Fig. 2. (color online) Stress σ_{11} along the line $x_1 = 0$.

To investigate the influence of the integration background cell to the solution accuracy, the boundary is approximated by two types of cells, i.e. a linear geometric representation, $\beta = 1$,

and a quadratic geometric representation, $\beta = 2$. Error

$$\varepsilon(v) = \sqrt{\frac{1}{N_t}\sum_{i=1}^{N_t}\left(v^{(i)} - v_h^{(i)}\right)^2}$$

is defined to evaluate the present method performance, where $v^{(i)}$ and $v_h^{(i)}$ refer to the values at the i-th test node obtained by the exact solutions and numerical method, respectively.

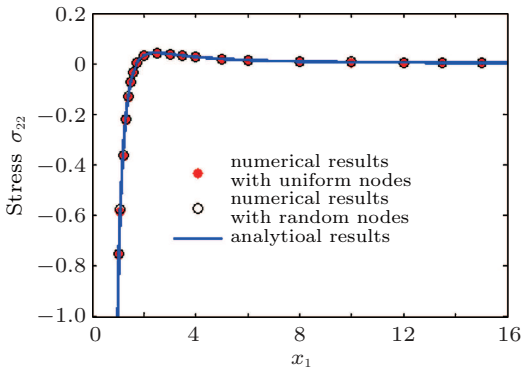


Fig. 3. (color online) Stress σ_{22} along the line $x_2 = 0$.

Figures 4 and 5 exhibit the error of displacement $\boldsymbol{u}$ and stress $\boldsymbol{\sigma}$, respectively. In this analysis, four different regular nodal arrangements of 16, 32, 64, and 128 nodes have been used. It can be seen that, as the number of boundary nodes increases, the error becomes smaller. According to the theoretical error results presented in Section 6, the theoretical convergence rates are 2 for $\beta = 1$ and 3 for $\beta = 2$. Both figures indicate that the experimental convergence rates approximate to the theoretical rates. Besides, stress $\boldsymbol{\sigma}$ and displacement $\boldsymbol{u}$ have almost the same experimental convergence rates. Therefore, the numerical results for this example are in good consistency with the theoretical error analysis.

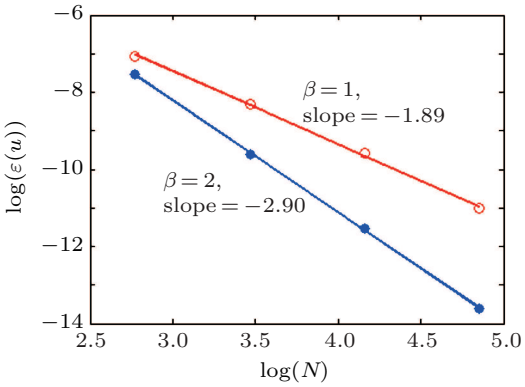


Fig. 4. (color online) Errors of the displacement $\boldsymbol{u}$.

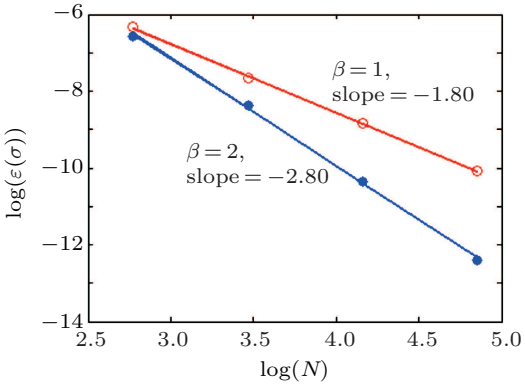


Fig. 5. (color online) Errors of the stress $\boldsymbol{\sigma}$.

8.2. Infinite cube with a spherical cavity

This problem consists of examining the stress distribution in the vicinity of a small cavity in an infinite cube subjected to far-field uniform tension, as illustrated in Fig. 6. The problem is solved for $a = 1$ and $\sigma_0 = 1$ with the material parameters, $E = 3.0 \times 10^7$ and $\nu = 0.3$.

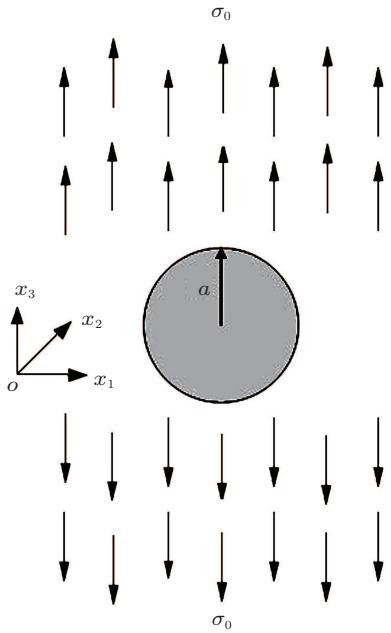


Fig. 6. An infinite cube with a spherical cavity subjected to a uniform tension.

The problem is solved for $a = 1$ and $\sigma_0 = 1$ with the material parameters, $E = 3.0 \times 10^7$ and $\nu = 0.3$. Figure 7 gives the comparison between the analytical solution and the numerical solution for the normal stress σ_{33} along the x_1 axis. It can be clearly seen that the numerical solution is in excellent agreement with the analytical ones.

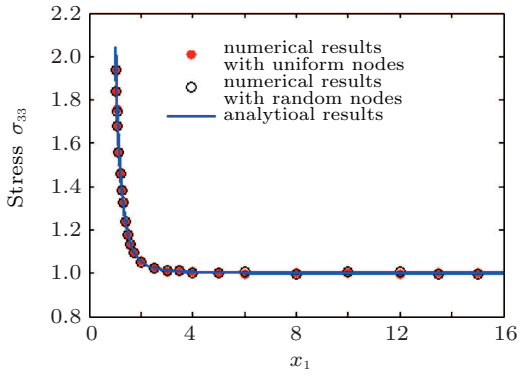


Fig. 7. (color online) Stress σ_{33} along the x_1 axis.

9. Conclusions

A meshless Galerkin method, known as the GBNM, has been developed in this paper for the numerical solution of infinite elastic solid mechanics problems. This Galerkin method reduces the computational dimensions of the original problem by one and thus gives a simple discretization of the infinite problems. The optimal asymptotic error estimates for both displacement and stress have been established in Sobolev spaces. The error study shows that the error bound of the numerical solution is directly related to the nodal spacing. Additionally, the error of displacement and stress hold the same order of convergence. Some examples have been given and the numerical results are accurate and are in good consistency with the theoretical analysis.

References

[1] Belytschko T, Lu Y Y and Gu L 1994 *Int. J. Numer. Methods Eng.* **37** 229
[2] Cheng R J and Cheng Y M 2011 *Chin. Phys. B* **20** 070206
[3] Wang J F, Sun F X and Cheng R J 2012 *Chin. Phys. B* **21** 090204
[4] Xia M H and Li J 2007 *Chin. Phys.* **16** 3067
[5] Chen L and Cheng Y M 2010 *Chin. Phys. B* **19** 090204
[6] Li Z H, Qin Y X and Cui X C 2012 *Acta Phys. Sin.* **61** 080205 (in Chinese)
[7] Liu M B and Chang J F 2010 *Acta Phys. Sin.* **59** 3654 (in Chinese)
[8] Zheng B J and Dai B D 2010 *Acta Phys. Sin.* **59** 5182 (in Chinese)
[9] Shirron J J and Babuska I 1998 *Comput. Methods Appl. Mech. Eng.* **164** 121
[10] Hsiao G C and Wendland W L 2008 *Boundary Integral Equations* (Berlin: Springer) pp. 45–75
[11] Zhu J and Yuan Z 2009 *Boundary Element Analysis* (Beijing: Science Press) p. 282 (in Chinese)
[12] Mukherjee Y X and Mukherjee S 1997 *Int. J. Numer. Methods Eng.* **40** 797
[13] Zhang J, Qin X, Han X and Li G 2009 *Int. J. Numer. Methods Eng.* **80** 320
[14] Cheng Y M and Peng M J 2005 *Sci. China: Phys. Mech. Astron.* **48** 641 (in Chinese)
[15] Ren H P, Cheng Y M and Zhang W 2010 *Sci. China: Phys. Mech. Astron.* **53** 758 (in Chinese)
[16] Chen S S, Li Q H and Liu Y H 2012 *Chin. Phys. B* **21** 110207
[17] Li X and Zhu J 2009 *J. Comput. Appl. Math.* **230** 314
[18] Li X and Zhu J 2009 *Comput. Methods Appl. Mech. Engrg.* **198** 2874
[19] Li X 2011 *Appl. Numer. Math.* **61** 1237
[20] Li X 2011 *Int. J. Numer. Methods Eng.* **88** 442
[21] Li X and Zhu J 2009 *CMES: Comput. Model. Eng. Sci.* **45** 1
[22] Li X 2012 *Eng. Anal. Bound. Elem.* **36** 993
[23] Cheng R J and Cheng Y M 2008 *Appl. Numer. Math.* **58** 884
[24] Cheng Y M and Li J H 2005 *Acta Phys. Sin.* **54** 4463 (in Chinese)
[25] Cheng Y M and Li J H 2006 *Sci. China: Phys. Mech. Astron.* **49** 46 (in Chinese)
[26] Li D M, Peng M J and Cheng Y M 2011 *Sci. China: Phys. Mech. Astron.* **41** 1003
[27] Bai F N, Li D M, Wang J F and Cheng Y M 2012 *Chin. Phys. B* **21** 020204
[28] Yang X L, Dai B D and Zhang W W 2012 *Chin. Phys. B* **21** 100208
[29] Cheng Y M, Li R X and Peng M J 2012 *Chin. Phys. B* **21** 090205
[30] Cheng Y M, Wang J F and Bai F N 2012 *Chin. Phys. B* **21** 090203
[31] Liew K M and Cheng Y M 2009 *Comput. Methods Appl. Mech. Eng.* **198** 3925